Critical properties of the Hintermann-Merlini model

Chengxiang Ding,[1,*] Yancheng Wang,[2] Wanzhou Zhang,[3] and Wenan Guo[4,†]
[1]*Department of Applied Physics, Anhui University of Technology, Maanshan 243002, China*
[2]*Beijing National Laboratory for Condensed Matter Physics, Institute of Physics, Chinese Academy of Sciences, Beijing 100190, China*
[3]*College of Physics and Optoelectronics, Taiyuan University of Technology, Shanxi 030024, China*
[4]*Department of Physics, Beijing Normal University, Beijing 100875, China*
(Received 8 August 2013; published 9 October 2013)

Many critical properties of the Hintermann-Merlini model are known exactly through the mapping to the eight-vertex model. Wu [J. Phys. C **8**, 2262 (1975)] calculated the spontaneous magnetizations of the model on two sublattices by relating them to the conjectured spontaneous magnetization and polarization of the eight-vertex model, respectively. The latter conjecture remains unproved. In this paper we numerically study the critical properties of the model by means of a finite-size scaling analysis based on transfer matrix calculations and Monte Carlo simulations. All analytic predictions for the model are confirmed by our numerical results. The central charge $c = 1$ is found for the critical manifold investigated. In addition, some unpredicted geometric properties of the model are studied. Fractal dimensions of the largest Ising clusters on two sublattices are determined. The fractal dimension of the largest Ising cluster on the sublattice A takes a fixed value $D_a = 1.888(2)$, while that for sublattice B varies continuously with the parameters of the model.

DOI: 10.1103/PhysRevE.88.042117 PACS number(s): 05.50.+q, 64.60.Cn, 64.60.De, 75.10.Hk

I. INTRODUCTION

The exact solutions [1,2] of the two-dimensional (2D) Ising model have significantly promoted the research of phase transitions and critical phenomena. Subsequently, the Ising model had become one of the most well-known lattice model in statistical physics. Another noted Ising system, the Baxter-Wu model [3], is defined on a triangular lattice with pure three-spin interactions. The model was proposed by Wood and Griffiths [4] and exactly solved by Baxter and Wu [3] by relating the model to the coloring problem on a honeycomb lattice. The solution gives the critical exponents $y_t = 3/2$ ($\alpha = 2/3$) and $y_h = 15/8$ ($\eta = 1/4$), which are exactly the same as those of the four-state Potts model [5,6], which can be derived via the Coulomb gas theory [7–9]. This means that the Baxter-Wu model belongs to the universality class of the four-state Potts model. The critical properties of the four-state Potts model are modified by logarithmic corrections [10,11] due to the second temperature field, which is marginally irrelevant [11,12]. With the two leading temperature fields simultaneously vanishing, the leading critical singularities of the Baxter-Wu model [13] do not have logarithmic factors. Deng *et al.* generalized the Baxter-Wu model in [13], where the spins are allowed to be q states (q can be larger than 2) and the up and down triangles can have different coupling constants. Both generalizations lead to discontinuous phase transitions.

Hintermann and Merlini [14] considered an Ising system on the Union Jack lattice (as shown in Fig. 1)

$$-\frac{H}{k_B T} = \sum_{\square} s(K_1\sigma_1\sigma_2 + K_2\sigma_2\sigma_3 + K_3\sigma_3\sigma_4 + K_4\sigma_4\sigma_1), \tag{1}$$

where the sum takes over all the square unit cells and K_i ($i = 1,2,3,4$) are the coupling constants. The model is similar to the Baxter-Wu model in the sense that both are Ising systems with pure three-spin interactions. However, the critical properties of the Hintermann-Merlini (HM) model are much more complicated. For the ferromagnetic case ($K_i > 0$), the model has fourfold degenerate ground states, as shown in Fig. 2. The nature of the phase transition breaking the Z_4 symmetry of the order parameter cannot be determined by the dimensionality of the system and the symmetry properties of the ground states [15]. The exponents may vary with some tuning parameter without changing the symmetry of the order parameter. Such behavior has been found, e.g., in the Ashkin-Teller model [16,17], the eight-vertex model [18,19], the 2D XY model in a fourfold anisotropic field [20], and the ferromagnetic Ising model with antiferromagnetic next-nearest-neighbor couplings on a square lattice [21–23].

Through mapping to the eight-vertex model [18,19], the free energy of the HM model has been found exactly [14]. The critical manifold and critical exponent y_t varying with the ratio of couplings were obtained. Based on the conjectured spontaneous magnetization [24] and the spontaneous polarization [25] of the eight-vertex model, Wu calculated the spontaneous magnetizations of the model on two sublattices. The results show that the two magnetizations possess different critical exponents [26]. The spontaneous magnetization of the eight-vertex model was derived later [27]; however, the spontaneous polarization remains a conjecture. It is thus necessary to verify the results numerically.

In present paper we study numerically the critical behavior of the ferromagnetic HM model with $K_1 = K_3 > 0$ and $K_2 = K_4 > 0$. The numerical procedure includes transfer matrix calculations and Monte Carlo simulations. The critical properties we study include not only the verification of the analytic predictions, but also the fractal structure of spin clusters.

The paper is organized in the following way. In Sec. II we summarize the theoretical results of the model. In Sec. III we introduce the transfer matrix method and present the associated numerical results. In Sec. IV we describe the algorithm used

*dingcx@ahut.edu.cn
†waguo@bnu.edu.cn

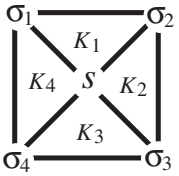

FIG. 1. Definition of the Hintermann-Merlini model. The lattice consists of two sublattices: The spin on sublattice A is denoted by σ and the spin on sublattice B is denoted by s. For a square unit cell, there are four spins σ_1, σ_2, σ_3, and σ_4 on sublattice A and one spin s on sublattice B.

in Monte Carlo simulations and give the associated numerical results. In Sec. V we define Ising clusters on two sublattices and numerically determine the fractal dimensions of the corresponding largest clusters, respectively. We summarize in Sec. VI.

II. EXACT SOLUTIONS

In this section we summarize the analytical results for the HM model [14,26]. Mapping of the model to vertex model can be accomplished by assigning arrows between the nearest-neighbor Ising spins of sublattice A (Fig. 3): If the two spins beside the arrow are the same, the arrow is rightward (or upward); otherwise it is leftward (or downward). There is a two-to-one correspondence between the Ising spin configurations and the arrow configurations.

After taking the sum over the spin s (in the center of the unit cell), the Boltzmann weights of the vertices are

$$\begin{aligned} a &= \cosh(K_1 + K_2 + K_3 + K_4), \\ b &= \cosh(K_1 - K_2 + K_3 - K_4), \\ c &= \cosh(K_1 - K_2 - K_3 + K_4), \\ d &= \cosh(K_1 + K_2 - K_3 - K_4). \end{aligned} \tag{2}$$

Thus the model is mapped to the symmetric eight-vertex model [18,19], which has been exactly solved by Baxter. For the ferromagnetic case considered in the present paper, the critical manifold is given by

$$a = b + c + d, \tag{3}$$

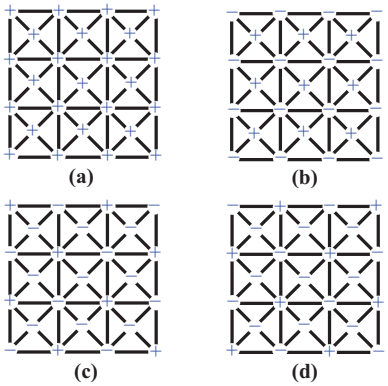

FIG. 2. (Color online) Four ground states of the ferromagnetic HM model.

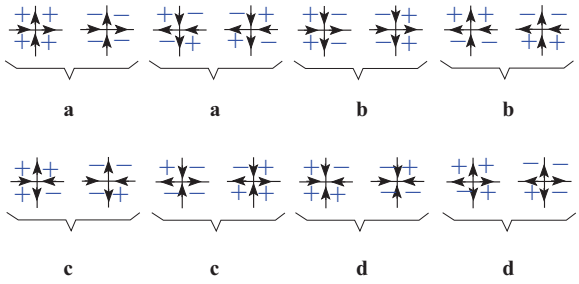

FIG. 3. (Color online) Mapping of the HM model to the eight-vertex model and the Boltzmann weights of the vertices. The Ising spins shown here are the spins on sublattice A, namely, the σ spins.

which leads to $K_c = \ln(1+\sqrt{2})/2$ for the uniform case ($K = K_1 = K_2 = K_3 = K_4$).

The singularity of the free energy density is governed by

$$f_{\text{sing}} \propto |T - T_c|^{\pi/u} \tag{4}$$

when $\pi/2u$ is not an integer (the case that $\pi/2u$ is an integer is not considered in the present paper). Here T_c is the critical temperature and $0 \leqslant u \leqslant \pi$ is given by [26]

$$\cos u = -\tanh\left[\frac{1}{2}\ln\frac{ab}{cd}\right]\Bigg|_{T_c} \quad \text{if} \quad a > b,c,d \text{ or } b > a,c,d, \tag{5}$$

$$\cos u = \tanh\left[\frac{1}{2}\ln\frac{ab}{cd}\right]\Bigg|_{T_c} \quad \text{if } d > a,b,c \text{ or } c > a,b,d. \tag{6}$$

For the ferromagnetic case that we consider, u is determined by (5). Since $f_{\text{sing}} \propto \xi^2$ and $\xi \sim |T - T_c|^{-1/y_t}$, the critical exponent y_t is thus found

$$y_t = \frac{2u}{\pi}. \tag{7}$$

For the uniform case, (7) gives $y_t = 4/3$.

A very interesting critical property of the HM model is that the spontaneous magnetizations M_A and M_B of sublattices A and B possess different critical exponents

$$M_A \propto (T_c - T)^{\beta_a}, \quad M_B \propto (T_c - T)^{\beta_b}. \tag{8}$$

The critical exponents β_a and β_b were obtained by Wu [26],

$$\beta_a = \frac{\pi}{16u}, \quad \beta_b = \frac{\pi - u}{4u}. \tag{9}$$

[It should be noted that the author switched the two critical exponents in Eq. (16) of [26].] According to the scaling law, this leads to two magnetic exponents y_{h1} and y_{h2},

$$\begin{aligned} y_{h1} &= 2 - \beta_a y_t = \frac{15}{8}, \\ y_{h2} &= 2 - \beta_b y_t = \frac{3\pi + u}{2\pi}. \end{aligned} \tag{10}$$

Here y_{h1} has a fixed value $15/8$, while y_{h2} varies continuously with the parameters of the model.

In following sections we will numerically study the critical properties of the model. The critical points and critical exponents will be numerically verified. In particular, Wu's result of β_b (y_{h2}) is based on the unproved conjecture of the spontaneous

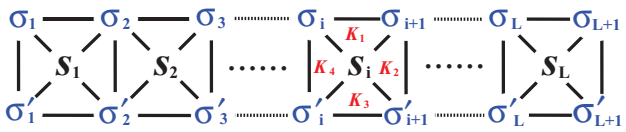

FIG. 4. (Color online) Definition of the row-to-row transfer matrix, where periodic boundary conditions are applied, namely, $\sigma_{L+1} = \sigma_1$ and $\sigma'_{L+1} = \sigma'_1$.

polarization [25] of the eight-vertex model, thus numerical verification is necessary. Our numerical studies are focused on the subspace that $K_1 = K_3 = K$ and $K_2 = K_4 = K'$. By defining $r \equiv K'/K$, the critical manifold and exponents are expressed as functions of r. It is worth noting that there is a symmetry for the transformation $r \to 1/r$. At a special point $r^* = 3.348\,258\,180\,5$ and its dual $1/r^* = 0.298\,662\,751\,2$, $u = 3\pi/4$, the analytic results give $y_t = 1/2, y_{h1} = 15/8 = y_{h2}$. This is the four-state Potts point.

III. TRANSFER MATRIX CALCULATIONS

As shown in Fig. 4, we define the row-to-row transfer matrix

$$\begin{aligned} T_{\vec{\sigma},\vec{\sigma}'} &= \sum_{\{s\}} \prod_{i=1}^{L} \exp[s_i(K_1\sigma_i\sigma_{i+1} + K_2\sigma_{i+1}\sigma'_{i+1} \\ &\quad + K_3\sigma'_{i+1}\sigma'_i + K_4\sigma'_i\sigma_i)] \\ &= 2^L \prod_{i=1}^{L} \cosh(K_1\sigma_i\sigma_{i+1} + K_2\sigma_{i+1}\sigma'_{i+1} \\ &\quad + K_3\sigma'_{i+1}\sigma'_i + K_4\sigma'_i\sigma_i), \end{aligned} \tag{11}$$

where $\vec{\sigma} = (\sigma_1, \sigma_2, \ldots, \sigma_L)$ and $\vec{\sigma}' = (\sigma'_1, \sigma'_2, \ldots, \sigma'_L)$ are the states of two neighboring rows, respectively. Here periodic boundary conditions are applied. For a system with M rows, the partition sum is found to be

$$Z = \mathrm{Tr}(T^M), \tag{12}$$

with the periodic boundary condition $\vec{\sigma}_{M+1} = \vec{\sigma}_1$ applied. In the limit $M \to \infty$, the free-energy density is determined by the leading eigenvalue Λ_0 of T

$$f = \frac{1}{L} \ln \Lambda_0. \tag{13}$$

For the HM model, the dimension of the matrix T is $d_T = 2^L$. To numerically calculate the eigenvalues of T, we use the sparse matrix technique, which sharply reduces the requirement of computer memory for storing the matrix elements. (For details of this technique, see [28–31].) We are able to calculate the eigenvalues of T with L up to 22. In our calculations, we restrict the system size L to even values because the ordered configurations, as shown in Fig. 2, do not fit well in odd systems.

The critical properties can be revealed by calculating three scaled gaps $X_i(K,L)$:

$$X_i(K,L) = \frac{1}{2\pi} \ln\left(\frac{\Lambda_0}{\Lambda_i}\right), \tag{14}$$

where Λ_i $(i = 1,2,3)$ are three subleading eigenvalues of the matrix T, respectively. According to the conformal invariance theory [32], the scaled gap $X_i(K,L)$ is related to a correlation length $\xi_i(K,L)$,

$$X_i(K,L) = \frac{L}{2\pi\xi_i(K,L)}, \tag{15}$$

where $\xi_i(K,L)$ governs the decay of a correlation function $G_i(r)$. According to the finite-size scaling [33], the gap in the vicinity of a critical point scales as

$$\begin{aligned} X_i(K,L) &= X_i + a_1(K - K_c)L^{y_t} + a_2(K - K_c)^2 L^{2y_t} \\ &\quad + \cdots + buL^{y_u} + \cdots, \end{aligned} \tag{16}$$

where X_i is the corresponding scaling dimension, which is related to an exponent $y_i = 2 - X_i$ according to the conformal invariance [32]. Here u is an irrelevant field and $y_u < 0$ is the corresponding irrelevant exponent; a_1, a_2, and b are unknown constants.

We focus on the energy-energy correlation $G_t(r)$ and two magnetic correlations $G_A(r)$ and $G_B(r)$. Generally speaking, the magnetic correlation function is defined as $G(r) = \langle s_0 s_r \rangle$. For the HM model, since the spontaneous magnetizations on the two sublattices behave differently, we examine two types of magnetic correlation functions: $G_A(r)$ with s_0 and s_r on the A sublattice and $G_B(r)$ on the B sublattice.

Let Λ_1 be the largest eigenvalue in the subspace that breaks the spin-up–spin-down symmetry, which means that the associated eigenvector $\vec{v}_1$ satisfies

$$\vec{v}_1 = -\mathbf{F}\vec{v}_1, \tag{17}$$

where $\mathbf{F}$ is the operator flipping spins. Thus the scaled gap $X_1(K,L)$ is identified as $X_{h1}(K,L)$ and the corresponding correlation is $G_A(r)$.

Let Λ_2 and Λ_3 be the second and third largest eigenvalues in the subspace keeping the spin-up–spin-down symmetry. It is not *a priori* clear which of the two corresponding gaps is the thermal one $X_t(K,L)$ or the magnetic one $X_{h2}(K,L)$. Based on the magnitudes of $X_t = 2 - y_t$ and $X_{h2} = 2 - y_{h2}$, we identify $X_2(K,L)$ and $X_3(K,L)$ as $X_{h2}(K,L)$ and $X_t(K,L)$, respectively.

Figures 5 and 6 illustrate $X_{h1}(K,L)$ and $X_{h2}(K,L)$ versus K in the uniform case, respectively. We then numerically solve

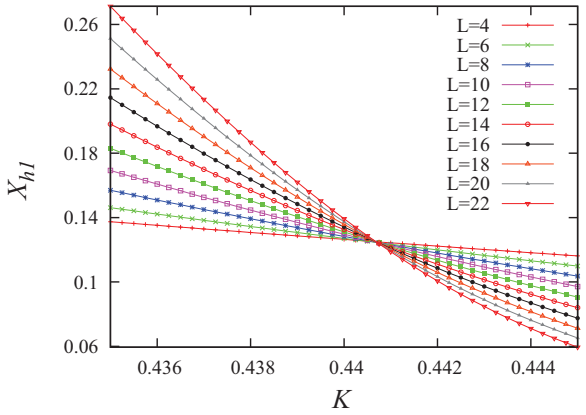

FIG. 5. (Color online) Scaled gap $X_{h1}(K,L)$ versus K for a sequence of system size L for the uniform HM model, whose critical point is $K_c = \ln(1+\sqrt{2})/2 = 0.440\,687$.

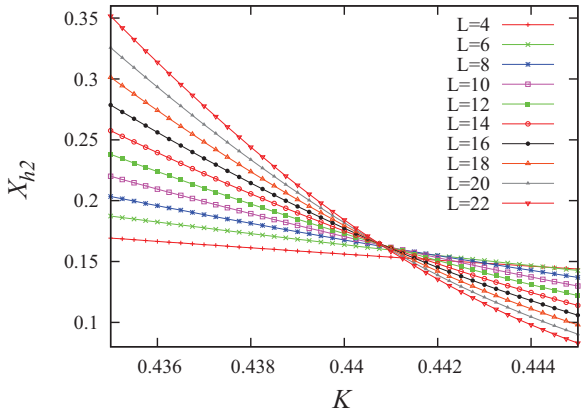

FIG. 6. (Color online) Scaled gap $X_{h2}(K,L)$ versus K for a sequence of system size L for the uniform HM model ($r = 1$), whose critical point is $K_c = \ln(1+\sqrt{2})/2 = 0.440\,687$.

the finite-size scaling equation

$$X_i(K,L) = X_i(K,L-2) \tag{18}$$

for $i = h1,h2$, respectively. The solution $K_c(L)$ satisfies

$$K_c(L) = K_c + auL^{y_u - y_t} + \cdots . \tag{19}$$

Here a is an unknown constant. Since $y_u < 0$ and $y_t \geqslant 0$, $K_c(L)$ converges to the critical point K_c with increasing system sizes. Equation (19) is used to determine the critical point in our numerical procedure. For the uniform case, we obtain $K_c = 0.440\,686\,79(5)$, which is in good agreement with the exact solution $K_c = \ln(1+\sqrt{2})/2$. We have also estimated the critical points of the cases with $r = K'/K = 2,3,4$, and 5, where $K = K_1 = K_3$ and $K' = K_2 = K_4$. Both $X_{h1}(K,L)$ and $X_{h2}(K,L)$ have been used to estimate the critical points; we list the best estimations in Table I. Our numerical estimations of K_c are consistent with the theoretical results to a high accuracy.

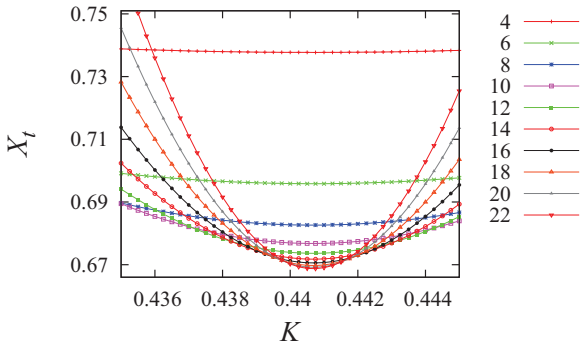

FIG. 7. (Color online) Scaled gap $X_t(K,L)$ versus K for a sequence of system size L for the uniform HM model ($r = 1$), whose critical point is $K_c = \ln(1+\sqrt{2})/2 = 0.440\,687$.

Exactly at the critical point K_c, (16) reduces to

$$X_i(K_c,L) = X_i + buL^{y_u} + \cdots , \tag{20}$$

which is used to determine the scaling dimensions X_{h1} and X_{h2}. For the uniform case $r = 1$, it gives $X_{h1} = 0.125\,000(1)$ and $X_{h2} = 0.1666\,66(1)$, which are consistent with the analytic results (Table I). We applied the same procedure to $r = 2,3,4,5$. The numerical estimations and the associated analytic results are consistent; see Table I.

We also calculate the scaled gap $X_t(K,L)$ in the vicinity of the critical point. The scaling behavior of $X_t(K,L)$ seems different from that of X_{h1} or X_{h2}, as shown in Fig. 7 for the uniform case. This is the result of $a_1 = 0$ in Eq. (16). The location of the minimum of $X_t(K,L)$ for a given L can be denoted as $K_c(L)$, which converges to the critical point K_c when $L \to \infty$. This property can also be used to estimate K_c, e.g., as was done in [34]; however, we do not do this in the present paper. By calculating $X_t(K,L)$ at the estimated K_c, we obtain the scaling dimension X_t according to (20). The results are listed in Table I.

TABLE I. Critical points, critical exponents, and scaling dimensions of the HM model. Here $r = K'/K$ (with $K = K_1 = K_3$ and $K' = K_2 = K_4$) and $r^* = 3.348\,258\,180\,5\ldots$. We use the following denotations: TP, theoretical predictions; MC, numerical results based on Monte Carlo simulations; and TM, numerical results based on transfer matrix calculations. The critical exponents and the scaling dimensions are related to $y_t = 2 - X_t$, $y_{h1} = 2 - X_{h1}$, and $y_{h2} = 2 - X_{h2}$.

r		1	2	3	r^*	4	5
K_c	TP	0.4406867935	0.3046889317	0.2406059125	0.225147108	0.2017629641	0.1751991102
	TM	0.44068679(5)	0.3046889(1)	0.2406059(1)	0.2251472(2)	0.2017629(1)	0.1751991(2)
y_t	TP	4/3	1.39668184	1.47604048	3/2	1.53960311	1.58921160
	MC	1.332(2)	1.397(2)	1.478(3)	1.500(1)	1.540(3)	1.590(2)
X_t	TP	2/3	0.60331816	0.52395952	1/2	0.46039689	0.41078840
	TM	0.66666(1)	0.603318(1)	0.52396(1)	0.50000(1)	0.46040(2)	0.41079(1)
y_{h1}	TP	15/8	15/8	15/8	15/8	15/8	15/8
	MC	1.874(1)	1.874(2)	1.876(2)	1.874(2)	1.877(3)	1.874(2)
X_{h1}	TP	1/8	1/8	1/8	1/8	1/8	1/8
	TM	0.125000(1)	0.125000(1)	0.125000(1)	0.12499(1)	0.12500(1)	0.12498(3)
y_{h2}	TP	11/6	1.84917046	1.86901012	15/8	1.88490078	1.89730290
	MC	1.833(1)	1.848(2)	1.870(2)	1.875(1)	1.886(2)	1.896(4)
X_{h2}	TP	1/6	0.15082954	0.13098988	1/8	0.11509922	0.10269710
	TM	0.166666(1)	0.150829(1)	0.130990(1)	0.12500(1)	0.115099(1)	0.102696(2)
c	TP	1	1	1	1	1	1
	MC	1.000000(1)	1.000000(1)	0.99998(3)	1.0000(1)	1.0000(2)	0.9999(1)

The finite-size-scaling behavior of the free-energy density at the critical point determines the central charge c according to [35,36]

$$f(L) \simeq f(\infty) + \frac{\pi c}{6L^2}. \tag{21}$$

Fitting the data of the free-energy density according to (21), we obtain the central charge $c = 1.000\,000(1)$ for the uniform case. For the other cases, the numerical estimations of the central charge are listed in Table I. The central charge for all r takes the fixed value $c = 1$, as expected for transitions breaking fourfold symmetry.

Furthermore, we consider the four-state Potts point $r = r^* = 3.348\,258\,180\,5\ldots$. A finite-size scaling analysis based on transfer matrix calculations is performed at this point. The numerical estimations obtained are listed in Table I. No logarithmic corrections are found, as in the Baxter-Wu model.

IV. MONTE CARLO SIMULATIONS

The Baxter-Wu model has been simulated by the Metropolis algorithm [37], the Wang-Landau algorithm [38], and a cluster algorithm [13,39]. The cluster algorithm is similar to the Swendsen-Wang algorithm [40] for the Potts model. In this algorithm, the triangular lattice is divided into three triangular sublattices. By randomly freezing the spins on one of the sublattices, the other two sublattices compose a honeycomb lattice with pair interactions; then a Swendsen-Wang-type algorithm can be formed to update the spins on this honeycomb lattice. In the present paper we suitably modify this cluster algorithm to simulate the HM model.

The algorithm is divided into three steps.

Step 1. Update the spins on sublattice A. Let the spins on sublattice B be unchanged (frozen) and the interactions of the spins on sublattice A reduce to pair interactions.

A. Bonds. A vertical (horizontal) edge on sublattice A belongs to two triangles. The interactions of the left (up) and right (down) triangles can be denoted by K_l and K_r, respectively, which may take the values K_1, K_2, K_3, or K_4. Place a bond on this edge with probability $p = 1 - e^{-2K_l - 2K_r}$ if the products of spins in both the left (up) triangle and the right (down) triangle are 1, $p = 1 - e^{-2K_l}$ if the product in only the left (upper) triangle is 1, $p = 1 - e^{-2K_r}$ if the product in only the right (down) triangle is 1, and $p = 0$ otherwise.

B. Clusters. A cluster is defined as a group of sites on sublattice A connected through the bonds.

C. Update spins. Independently flip the spins of each cluster with probability 1/2.

Step 2. Update the spins on sublattice B and half of the spins on sublattice A. This step is very similar to step 1, but we freeze only half of the spins on sublattice A, which are labeled A_1 (Fig. 8). The other spins (on sublattice $B + A_2$) are updated, whose interactions also reduce to pair interactions when A_1 spins are frozen.

Step 3. Update the spins on sublattice B and the other half of the spins on sublattice A. In this step, the spins labeled A_2 (in Fig. 8) are frozen and the other spins (on sublattice $B + A_1$) are updated.

In a complete sweep, all the spins are updated twice.

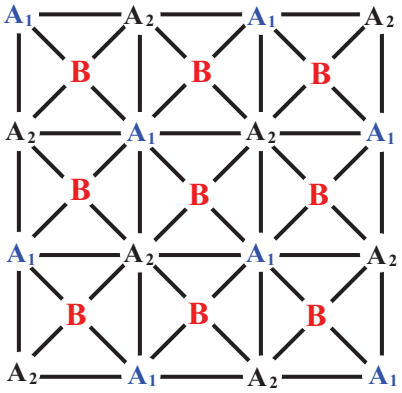

FIG. 8. (Color online) When B spins are frozen, the interactions of A spins (A_1 and A_2 spins) reduce to pair interactions; when A_1 spins are frozen, the interactions of $B + A_2$ spins reduce to pair interactions; when A_2 spins are frozen, the interactions of $B + A_1$ spins reduce to pair interactions.

In the simulations, the sampled variables include the specific heat C and the magnetizations M_A on sublattice A and M_B on sublattice B. The specific heat is calculated from the fluctuation of energy density E,

$$C = \frac{L^2(\langle E^2\rangle - \langle E\rangle^2)}{k_B T^2}, \tag{22}$$

where L is the linear size of the system and angular brackets denote the ensemble average. The magnetizations are defined as

$$M_A = \frac{\left\langle \left| \sum_{i=1}^{N} \sigma_i \right| \right\rangle}{N}, \tag{23}$$

$$M_B = \frac{\left\langle \left| \sum_{i=1}^{N} s_i \right| \right\rangle}{N}, \tag{24}$$

where $N = L^2$ is the number of total sites on sublattice A or B.

In order to demonstrate our numerical procedure based on the Monte Carlo simulations, we take the uniform case ($K = K_1 = K_2 = K_3 = K_4$) as an example. The cluster algorithm is very efficient, which easily allows us to do meaningful simulations for the system with linear size up to $L = 384$. All the simulations are performed at the critical point K_c. After equilibrating the system, 10^7 samples were taken for each system size. Using the Levenberg-Marquardt algorithm, we fit the data of C according to the finite-size scaling formula [33]

$$C(L) = C_0 + L^{2y_t - d}(a + bL^{y_1}), \tag{25}$$

where bL^{y_1} is the leading correction-to-scaling term with $y_1 < 0$ the leading irrelevant exponent. Here $d = 2$ is the dimensionality of the lattice and C_0, a, and b are unknown parameters. The fitting yields $y_t = 1.332(2)$, which is in good agreement with the exact result $y_t = 4/3$.

The finite-size scaling behaviors of the magnetizations M_A and M_B are

$$M_A = L^{y_{h1} - d}(a + bL^{y_1}), \tag{26}$$

$$M_B = L^{y_{h2} - d}(a' + b'L^{y_1'}), \tag{27}$$

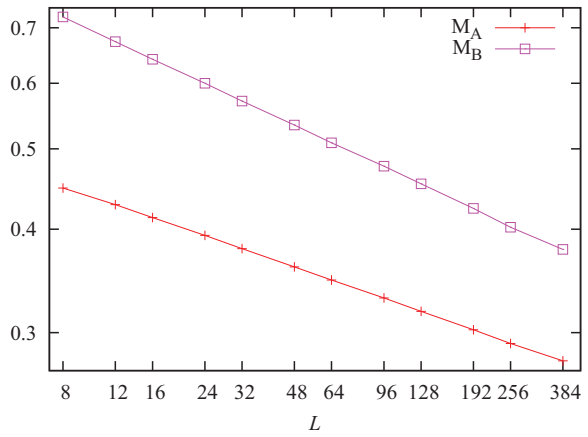

FIG. 9. (Color online) A log-log plot of the magnetizations M_A and M_B versus system size L for the HM model at the critical point $K_c = \ln(1+\sqrt{2})/2$ for the uniform case ($K = K_1 = K_2 = K_3 = K_4$).

respectively. A log-log plot of M_A and M_B versus L is shown in Fig. 9. The fits yield $y_{h1} = 1.874(1)$ and $y_{h2} = 1.833(1)$, where y_{h1} and y_{h2} are in good agreement with the analytic predictions $y_{h1} = 15/8$ and $y_{h2} = 11/6$, respectively.

We also simulate the $r = 2, 3, 4, 5$, and r^* cases. The numerical estimations of y_t, y_{h1}, y_{h2} and the corresponding analytic predictions are listed in Table I. They are in good agreement. In these fits, no logarithmic corrections to scaling are found.

V. FRACTAL STRUCTURE OF THE MODEL

In addition to calculating the critical exponents y_t, y_{h1}, and y_{h2}, we also investigate the geometric properties of the model. The configurations of the HM model are represented by Ising spins. Thus we can define Ising clusters for the model as in the Ising model [41]. To do so, each sublattice is viewed as a square lattice. For two nearest-neighbor Ising spins on a sublattice, they are considered to be in the same cluster if they have the same sign. Here, by "nearest neighbor" we

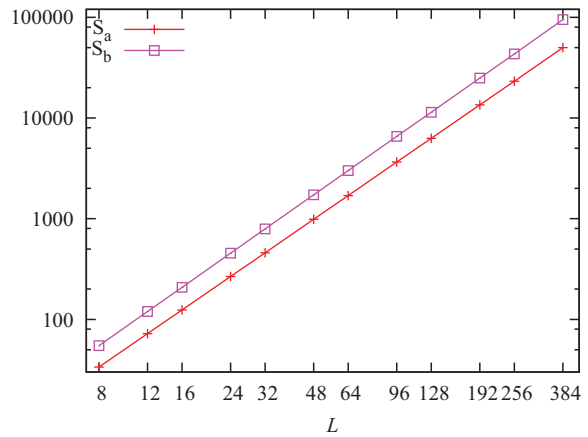

FIG. 10. (Color online) A log-log plot of S_a and S_b versus system size L for the HM model at the critical point $K_c = \ln(1+\sqrt{2})/2$ for the uniform case ($K = K_1 = K_2 = K_3 = K_4$).

TABLE II. Fractal dimensions of the HM model. Here D_a is the fractal dimension of the A cluster, D_b is the fractal dimension of the B cluster, $r = K'/K$ (with $K = K_1 = K_3$ and $K' = K_2 = K_4$), and $r^* = 3.348\,258\,180\,5$.

r	1	2	3	r^*	4	5
D_a	1.888(1)	1.889(1)	1.890(3)	1.889(2)	1.888(1)	1.888(2)
D_b	1.925(1)	1.931(1)	1.939(1)	1.941(1)	1.945(2)	1.951(2)

mean that the neighborhood of the site is the same as that of a site in a square lattice. This definition is applied to the two sublattices respectively, thus there are two types of Ising clusters. For clarity, we call the Ising cluster on sublattice A the A cluster and the Ising cluster on sublattice B the B cluster.

The simulations are also performed at the critical points. The sizes of the largest A cluster and the largest B cluster are denoted by S_a and S_b, respectively. They satisfy the finite-size scaling

$$S_a = L^{D_a}(a + bL^{y_1}), \tag{28}$$

$$S_b = L^{D_b}(a' + b'L^{y_1'}), \tag{29}$$

which means that the largest A cluster and the largest B cluster are fractals, with D_a and D_b the fractal dimensions, respectively. Figure 10 is an illustration of S_a and S_b versus system size L for the uniform case. Fitting the data according to (28) and (29), we find $D_a = 1.888(1)$ and $D_b = 1.925(1)$.

The same procedure was applied to $r = 2, 3, 4, 5$, and r^*. The results obtained are listed in Table II. The fractal dimension of the A cluster has a fixed value $D_a = 1.888(2)$, while that of the B cluster varies with the ratio r.

VI. CONCLUSION

We have numerically studied the critical properties of the HM model by means of finite-size scaling analysis based on the transfer matrix calculations and Monte Carlo simulations. For the critical points and the critical exponents y_t (X_t), y_{h1} (X_{h1}), and y_{h2} (X_{h2}), our numerical estimations are in good agreement with the corresponding analytic predictions [14,26]. The analytic prediction for y_{h2} is based on the conjectured spontaneous polarization of the eight-vertex model, which remains unproved. Our numerical results verified the correctness of the prediction.

In addition, the central charge of the model was found to be $c = 1$. This is consistent with the fact that $y_{h1} = 15/8$ and y_t and y_{h2} vary continuously with the parameters, which is related to the fourfold degeneracy of the ground states of the model. Usually, logarithmic corrections [10,23,42] show up in the four-state Potts point for the model with fourfold degenerate ground states due to the second temperature field. However, we did not see such logarithmic corrections in the four-state Potts point of the HM model. This is the same as the Baxter-Wu model, in which the amplitude of the marginally irrelevant operator is zero.

Furthermore, two unpredicted critical exponents were found to describe geometric properties of the model. We

defined clusters based on the Ising spin configurations on the two sublattices of the model. The fractal dimension of the largest cluster on sublattice A takes the fixed value $D_a = 1.888(2)$, while the fractal dimension of the largest cluster on sublattice B varies continuously with the parameters of the model.

ACKNOWLEDGMENT

C.D. thanks F. Y. Wu for valuable discussion regarding the analytical results of the HM model. This work was supported by the National Science Foundation of China under Grant Nos. 11205005 (C.D.) and 11175018 (W.G.).

[1] L. Onsager, Phys. Rev. **65**, 117 (1944).
[2] C. N. Yang, Phys. Rev. **85**, 808 (1952).
[3] R. J. Baxter and F. Y. Wu, Phys. Rev. Lett. **31**, 1294 (1973).
[4] D. W. Wood and H. P. Griffiths, J. Phys. C **5**, L253 (1972).
[5] R. B. Potts, Proc. Cambridge Philos. Soc. **48**, 106 (1952).
[6] F. Y. Wu, Rev. Mod. Phys. **54**, 235 (1982).
[7] M. P. M. den Nijs, J. Phys. A **12**, 1857 (1979).
[8] M. P. M. den Nijs, Phys. Rev. B **27**, 1674 (1983).
[9] B. Nienhuis, J. Stat. Phys. **34**, 731 (1984).
[10] J. Salas and A. D. Sokal, J. Stat. Phys. **88**, 567 (1997).
[11] M. Nauenberg and D. J. Scalapino, Phys. Rev. Lett. **44**, 837 (1980).
[12] B. Nienhuis, A. N. Berker, E. K. Riedel, and M. Schick, Phys. Rev. Lett. **43**, 737 (1979).
[13] Y. Deng, W.-A. Guo, J. R. Heringa, H. W. J. Blöte, and B. Neinhuis, Nucl. Phys. B **827**, 406 (2010).
[14] A. Hintermann and D. Merlini, Phys. Lett. A **41**, 208 (1972).
[15] M. Suzuki, Prog. Theor. Phys. **51**, 1992 (1974).
[16] J. Ashkin and E. Teller, Phys. Rev. **64**, 178 (1943).
[17] S. Wiseman and E. Domany, Phys. Rev. E **48**, 4080 (1993).
[18] R. J. Baxter, Phys. Rev. Lett. **26**, 832 (1971).
[19] R. J. Baxter, *Exactly Solved Models in Statistical Mechanics* (Academic, London, 1982).
[20] J. V. José, L. P. Kadanoff, S. Kirkpatrick, and D. R. Nelson, Phys. Rev. B **16**, 1217 (1977).
[21] M. P. Nightingale and H. W. J. Blöte, Physica A **251**, 211 (1998).
[22] S. Jin, A. Sen, and A. W. Sandvik, Phys. Rev. Lett. **108**, 045702 (2012).
[23] S. Jin, A. Sen, W.-A. Guo, and A. W. Sandvik, Phys. Rev. B **87**, 144406 (2013).
[24] M. N. Barber and R. J. Baxter, J. Phys. C **6**, 2913 (1973).
[25] R. J. Baxter and S. B. Kelland, J. Phys. C **7**, L403 (1974).
[26] F. Y. Wu, J. Phys. C **8**, 2262 (1975).
[27] R. J. Baxter, J. Stat. Phys. **15**, 485 (1976).
[28] H. W. J. Blöte and M. P. Nightingale, Physica A (Amsterdam) **112**, 405 (1982).
[29] H. W. J. Blöte and B. Nienhuis, J. Phys. A **22**, 1415 (1989).
[30] H. W. J. Blöte and M. P. Nightingale, Phys. Rev. B **47**, 15046 (1993).
[31] X. F. Qian, M. Wegewijs, and H. W. J. Blöte, Phys. Rev. E **69**, 036127 (2004).
[32] J. L. Cardy, in *Phase Transitions and Critical Phenomena*, edited by C. Domb and J. L. Lebowitz (Academic, London, 1987), Vol. 11, p. 55, and references therein.
[33] For reviews see, e.g., M. P. Nightingale, in *Finite-Size Scaling and Numerical Simulation of Statistical Systems*, edited by V. Privman (World Scientific, Singapore 1990); also see M. N. Barber, in *Phase Transitions and Critical Phenomena*, edited by C. Domb and J. L. Lebowitz (Academic, New York, 1983), Vol. 8.
[34] H. W. J. Blöte and M. P. Nightingale, Physica A (Amsterdam) **129**, 1 (1984).
[35] H. W. J. Blöte, J. L. Cardy, and M. P. Nightingale, Phys. Rev. Lett. **56**, 742 (1986).
[36] I. Affleck, Phys. Rev. Lett. **56**, 746 (1986).
[37] L. N. Shchur and W. Janke, Nucl. Phys. B **840**, 491 (2010).
[38] N. Schreiber and J. Adler, J. Phys. A **38**, 7253 (2005).
[39] H. W. J. Blöte, J. R. Heringa, and E. Luijten, Comput. Phys. Commun. **147**, 58 (2002).
[40] R. H. Swendsen and J. S. Wang, Phys. Rev. Lett. **58**, 86 (1987).
[41] W. Janke and A. M. J. Schakel, Phys. Rev. E **71**, 036703 (2005).
[42] J.-P. Lv, Y. Deng, and Q.-H. Chen, Phys. Rev. E **84**, 021125 (2011).